Reconstructing an Interdecadal Pacific Oscillation Index from a Pacific Basin–Wide Collection of Ice Core Records🖉

STACY E. PORTER,[a] ELLEN MOSLEY-THOMPSON,[a,b] LONNIE G. THOMPSON,[a,c] AND AARON B. WILSON[a,d]

[a] *Byrd Polar and Climate Research Center, The Ohio State University, Columbus, Ohio*
[b] *Department of Geography, The Ohio State University, Columbus, Ohio*
[c] *School of Earth Sciences, The Ohio State University, Columbus, Ohio*
[d] *College of Food, Agricultural, and Environmental Sciences, Ohio State University Extension, The Ohio State University, Columbus, Ohio*

ABSTRACT: Using an assemblage of four ice cores collected around the Pacific basin, one of the first basinwide histories of Pacific climate variability has been created. This ice core–derived index of the interdecadal Pacific oscillation (IPO) incorporates ice core records from South America, the Himalayas, the Antarctic Peninsula, and northwestern North America. The reconstructed IPO is annually resolved and dates to 1450 CE. The IPO index compares well with observations during the instrumental period and with paleo-proxy assimilated datasets throughout the entire record, which indicates a robust and temporally stationary IPO signal for the last ~550 years. Paleoclimate reconstructions from the tropical Pacific region vary greatly during the Little Ice Age (LIA), although the reconstructed IPO index in this study suggests that the LIA was primarily defined by a weak, negative IPO phase and hence more La Niña–like conditions. Although the mean state of the tropical Pacific Ocean during the LIA remains uncertain, the reconstructed IPO reveals some interesting dynamical relationships with the intertropical convergence zone (ITCZ). In the current warm period, a positive (negative) IPO coincides with an expansion (contraction) of the seasonal latitudinal range of the ITCZ. This relationship is not stationary, however, and is virtually absent throughout the LIA, suggesting that external forcing, such as that from volcanoes and/or reduced solar irradiance, could be driving either the ITCZ shifts or the climate dominating the ice core sites used in the IPO reconstruction.

KEYWORDS: Pacific Ocean; Paleoclimate; Multidecadal variability

1. Introduction

Over the twentieth century, Pacific climate and ecology have experienced several regime shifts (Mantua et al. 1997; Minobe 1997; Zhang et al. 1997; Overland et al. 1999; Bond et al. 2003; Deser et al. 2004). Mantua et al. (1997) defined this multidecadal variability as the Pacific decadal oscillation (PDO) based on the oscillation of North Pacific sea surface temperatures (SSTs) between warm and cold regimes about every 20–30 years. The PDO shares a similar SST signature with the interdecadal Pacific oscillation (IPO; Folland et al. 1999; Power et al. 1999), a Pacific basin–wide signal of SST variability. Figure 1 shows the SST and sea level pressure anomalies associated with a positive phase of IPO including warmer waters in the eastern equatorial Pacific and along the west coast of North America. Many authors suggest that the PDO and the IPO are comparable in describing Pacific climate variability (Folland et al. 2002; Deser et al. 2004; Dong and Dai 2015); therefore, Pacific decadal variability (PDV) is used here to encompass both phenomena.

The multidecadal shifts in the background state of the Pacific Ocean have both global and regional ramifications. PDV has been shown to influence global surface temperature such that periods of rapid warming are associated with warm/positive phases of PDV and periods of reduced rates of warming are associated with cold/negative phases of PDV (Meehl et al. 2013; Kosaka and Xie 2016; Henley and King 2017). The relationship between global surface temperatures and PDV is consistent on decadal and interdecadal time scales but is less consistent on shorter time scales (Sankaran 2017). On the regional scale, PDV modulates the influence of El Niño–Southern Oscillation (ENSO) on temperature and precipitation (Gershunov and Barnett 1998; Hu and Huang 2009; Wang et al. 2014; Westra et al. 2015; Dong et al. 2018). On the contrary, others suggest ENSO events establish PDV by subtropical stochastic processes, such that PDV is the reddened, autocorrelative response to ENSO (Shakun and Shaman 2009; Di Lorenzo et al. 2015). To better predict, as well as hindcast, the impacts of ENSO on global climate, it is essential to ascertain the background state of PDV.

Understanding the drivers of the multidecadal behavior of the Pacific Ocean is crucial for future climate projections, but current understanding of this behavior is limited due to relatively short observational records. Other methods are thus required such as modeling and using paleoclimate proxy data. Indeed, several studies, based primarily on tree ring data, have attempted to reconstruct the long-term behavior of PDO. These include data from North America (Biondi et al. 2001;
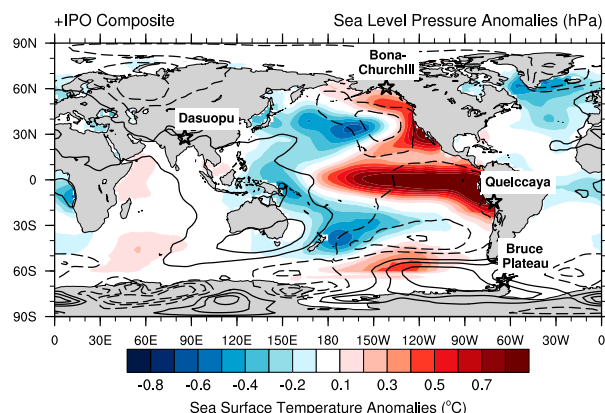
FIG. 1. Composite of observed positive IPO (tripole IPO > 0.75; Henley 2015) anomalies (base period: 1981–2010) for sea surface temperature (shading) and sea level pressure (0.5-hPa contours; negative contours are dashed) from NCEP–NCAR (1996) reanalysis. The drill site locations for the four ice cores used in this study are shown.

D'Arrigo et al. 2001; Gedalof and Smith 2001; MacDonald and Case 2005) and East Asia (D'Arrigo and Wilson 2006). Historical drought/flood records from eastern China have also been used for PDO reconstructions (Shen et al. 2006). Vance et al. (2015) created a millennial IPO reconstruction based on annual accumulation and sea salt concentrations from the Law Dome ice core in East Antarctica. Linsley et al. (2008) created a ~350-yr IPO reconstruction using oxygen isotopic ratios from five South Pacific coral records. Little agreement exists among these reconstructions prior to the twentieth century (Wise 2015; Henley 2017) likely due in part to their limited geographical extent. Buckley et al. (2019) created one of the first trans-Pacific IPO reconstructions by including tree ring samples from Vietnam and the North American Drought Atlas. This current study uses readily available ice core records from four separate regions around the Pacific Ocean including the tropics and high latitudes (Fig. 1) to construct a basinwide history of Pacific climate variability. The individual ice core records used in this study and the reconstruction methodology are discussed in section 2. In section 3, the characteristics of the ice core–derived reconstruction are discussed and validated by observations, paleo-proxy assimilated products, and previous reconstructions of Pacific climate variability. Further exploration of the Pacific variability and possible drivers during the Little Ice Age are included in section 4, and the main conclusions are summarized in section 5.

2. Data and methods

a. Ice core records

For more than 40 years, the Ice Core Paleoclimatology Group at the Byrd Polar and Climate Research Center has retrieved and preserved a worldwide collection of ice cores. Each ice core has been analyzed to determine net annual accumulation (A_n), insoluble dust concentrations, and the stable oxygen isotopic ratio ($\delta^{18}O$), which typically serves as a proxy

for temperature. The specific ice core records from South America, Tibetan Plateau, Antarctic Peninsula, and southeast Alaska (Fig. S1 in the online supplemental material) were chosen because previous research has established that each ice core record exhibits a signal of Pacific climate variability on either interannual or decadal time scales. Each core is annually resolved to at least 1450 CE, and the autocorrelative and spectral features of each record are shown in Figs. S2 and S3, respectively. Their unique signatures of Pacific climate variability are described below.

In 2003, an ice core was retrieved from the summit of the Quelccaya ice cap [13.93°S, 70.83°W; 5670 m above mean sea level (MSL)] situated in the southern Peruvian Andes (Fig. 1). Thompson et al. (2013) demonstrated the remarkable reproducibility of the results from the Quelccaya site between ice cores drilled in 1983 and 2003, as well as the spatial similarities between the Summit and North Domes, suggesting a high signal-to-noise ratio in the $\delta^{18}O$ and accumulation records. Thompson et al. (2013, 2017) demonstrated that the annually resolved $\delta^{18}O$ record is related to SSTs in the Niño-3 and Niño-4 regions of the Pacific despite its primary Atlantic basin moisture source. Net accumulation (A_n) reflects changes in regional Amazonian rainfall as well as latitudinal shifts in the position of the intertropical convergence zone (ITCZ). The $\delta^{18}O$ record likely reflects the westerly wind anomalies associated with a warm equatorial Pacific (Vuille et al. 2003). However, the magnitude, spatial structure, and timing of ENSO-related precipitation anomalies in South America vary with the phase of PDV (Andreoli and Kayano 2005; Wang et al. 2014). Thus, the Quelccaya ice core, through its relationship with equatorial Pacific SSTs, elucidates ENSO history and represents the eastern equatorial region of the Pacific basin.

On the western side of the Pacific, ENSO events, and their modulation of the Walker circulation, influence the monsoon systems over Asia and India (Ropelewski and Halpert 1987), although the ENSO influence has not been consistent (Kumar et al. 2006). PDV modulates ENSO effects on the Indian monsoon such that an El Niño (a La Niña) event under a warm/positive (cold/negative) PDV phase weakens (strengthens) the monsoon to a greater extent than when ENSO and PDV are out of phase (Krishnan and Sugi 2003; Wang et al. 2014). Warm/positive PDV conditions initiate persistently dry periods in the Indian monsoon region and contribute to "megadroughts" (Meehl and Hu 2006). In 1997, an ice core was drilled from the Dasuopu glacier (28.38°N, 85.71°E; 7200 m MSL) in the Himalaya along the southern Tibetan Plateau (Fig. 1). The Dasuopu ice core was drilled to bedrock (~167.7 m) and is annually resolved to 1440 CE with an annual net accumulation of about 1.0 m water equivalent (Thompson et al. 2000). The $\delta^{18}O$ record from Dasuopu exhibits a pronounced upward trend coincident with the current warming trend. The $\delta^{18}O$ and dust records are positively correlated (see Table S1 in the online supplemental material), and $\delta^{18}O$ enrichment is observed during the extreme drought period beginning ~1790 CE (Thompson et al. 2000). A contemporaneous drought is also documented in Quelccaya ice core records (Thompson et al. 2018). Accumulation, dust, and chloride

concentrations represent the strength of the monsoon and drought events (Thompson et al. 2000) as the Indian summer monsoon serves as a primary precipitation source over South Asia and inland over the Himalaya and southern Tibetan Plateau. Thus, the Dasuopu ice core is excellently situated to provide the western Pacific perspective of PDV.

Interannual ENSO variability influences the orientation of the South Pacific convergence zone (SPCZ), a band of convection extending from New Guinea to French Polynesia (Vincent 1994). Energy stemming from the SPCZ is transferred poleward by transient eddies, and this process enhances cyclonic activity around Antarctica (Chen et al. 1996). ENSO variability thereby influences the Antarctic Peninsula through shifts in the position of the SPCZ. On longer time scales, PDV also modulates the position of the SPCZ (Salinger et al. 2001; Folland et al. 2002) and hence, cyclonic activity in the Amundsen Sea low region (Fig. 1). Through Rossby wave trains, PDV influences the surface heating rates over West Antarctic and basal heating rates under the Ross Ice Shelf (Clem et al. 2018). PDV also affects convective heating over the eastern equatorial Pacific which has been linked to Antarctic sea ice extent (Meehl et al. 2016). Goodwin et al. (2016) demonstrated the influence of Pacific climate variability on the Antarctic Peninsula using an accumulation record from the Bruce Plateau ice core. This core was recovered to bedrock (448.12 m) in 2010 from the Bruce Plateau ice field on the Antarctic Peninsula (66.03°S, 64.07°W; 1975.5 m MSL). Tropical Pacific variability imparts a greater influence on Bruce Plateau accumulation during cold/negative PDV phases when the SPCZ is shifted southwestward (Goodwin et al. 2016). The interaction between tropical Pacific variability and the strength of the circumpolar westerlies described by the southern annular mode has been shown to influence the climate of the Antarctic Peninsula (Clem and Fogt 2013). Hence, PDV also controls the relationship between Bruce Plateau accumulation and the southern annular mode (Goodwin et al. 2016), thereby demonstrating the far afield effects PDV has on global climate.

PDV in the North Pacific manifests as shifts in the SST patterns with a dipole between the central North Pacific and a horseshoe-shaped pattern along the western coast of North America. Changes in the overlying atmospheric pressure including the Aleutian low (Fig. 1), a semi-permanent low pressure system over the central North Pacific, accompany this horseshoe-shaped SST pattern. The strength and position of the Aleutian low ultimately influence the temperature and precipitation over northwestern North America. In 2002, the 460 m Bona–Churchill ice core was retrieved to bedrock from the col between Mount Bona and Mount Churchill in the Wrangell–St. Elias Mountain Range (61.4°N, 141.7°W; 4420 m MSL) in southeastern Alaska. The δ^{18}O record from Bona–Churchill reflects changes in the climate over the Bering Sea (Porter et al. 2019), which is strongly influenced by the strength and position of the Aleutian low.

b. Observational and reanalyzed data

The observed IPO index used in this study for calibration, comparison, and validation is based on SST anomalies in three centers of action in the Pacific Ocean that create a tripole index (Henley 2015; Henley et al. 2015). The NCEP–NCAR gridded reanalysis is used for climate variables in the instrumental period (Kalnay et al. 1996; NCEP–NCAR 1996). Observed precipitation data for the satellite era (post-1979) are from the Global Precipitation Climatology Project v2.3 (Adler et al. 2018; GPCP 2016). The observed monthly Palmer Drought Severity Index (PDSI) spans a global 2.5° grid (Dai et al. 2004; Dai 2017). Paleo-proxy data assimilations are included in this study to validate the ice core–derived reconstruction of Pacific climate variability. These include the Paleo Hydrodynamics Data Assimilation (PHYDA 2018) product from Steiger et al. (2018) and the Last Millennium Reanalysis (LMR 2019) v2.0 (Tardif et al. 2019; Anderson et al. 2019) and v2.1 (Tardif et al. 2019). PHYDA provides 2-m temperature and PDSI on a 2° grid by combining nearly 3000 proxy data series and modeled output from the Community Earth System Model Last Millennium Ensemble (Otto-Bliesner et al. 2016). The PHYDA product also includes the latitudinal location of the ITCZ in 11 longitudinal zones and the equatorial Pacific zonal SST gradient. LMR v2.1 assimilates the PAGES 2k Consortium (2017) proxy network with both climate and proxy system modeling (Tardif et al. 2019). LMR v2.0 includes 2290 additional proxy records, comprising mostly tree ring chronologies (Anderson et al. 2019). Output data from LMR v2.0 and v2.1 include annually resolved surface air and sea temperature, sea level pressure, 500-hPa geopotential height, precipitation, precipitable water, and PDSI, all on a 2° grid, as well as time series for various climate indices (e.g., PDO, Niño-3.4, Atlantic multidecadal oscillation, etc.) (LMR 2019). It should be noted that the PHYDA and LMR products contain considerable overlap in their proxy networks, and the δ^{18}O records from the Quelccaya and Dasuopu ice cores are included in both networks.

c. Principal component regression

Principal component regression (PCR) reduces the ice core variables to their principal components, which reduces the number of variables for inclusion into a model and accounts for collinearity under the presumed independence of principal component analysis. Mann et al. (1998) employed this method to examine global temperature patterns with a multiproxy network of paleoclimate data, and later Mann et al. (2008) demonstrated its robustness among various reconstruction methods. The annual average oxygen isotopic ratio, net accumulation, and dust concentration records from each of the four ice cores from 1900 to 1996 (their post-1900 period of overlap) were used in the principal component analysis. The data were pretreated by linearly detrending each record over its entire length. The 1600 CE eruption of Huaynaputina strongly impacted the Quelccaya dust record; thus, the 8 years following the eruption that exhibited dust concentrations exceeding the mean by more than two standard deviations were removed. The oxygen isotope records exhibit a normal distribution, and a natural log transformation was performed on the dust and accumulation records to achieve normality. The Dasuopu dust record did not achieve normality with a natural log

transformation; therefore, a square root transformation was performed for this record.

These pretreated records were subjected to a rotated varimax principal component analysis using SPSS. Five factors explaining a total of 57% of the variance were extracted from the ice core records while random time series with the same statistical moments only explained ~47% of the total variance. Each factor individually explains 9.5%–13.4% of the variance (Table S2) and not surprisingly, some factors are strongly influenced by individual ice core site variables. For example, factors 1 and 2 are heavily weighted in the Bruce Plateau and Dasuopu records, respectively. The remaining three factors represent combinations of variables from Quelccaya, Bona–Churchill, Bruce Plateau, and to a lesser extent, Dasuopu.

Correlation coefficients were calculated between the five principal components (PCs) and the annual and seasonal IPO indices determined by the tripole index from Henley et al. (2015) for the 1900–96 CE period, given uncertainties in the observational network prior to the twentieth century. For the IPO, the strongest correlations are for the annual (calendar year) IPO. Since Dasuopu, Bona–Churchill, and Quelccaya are dated as thermal years (July–June), an inherent lag exists when their records are compared with the January–December IPO, such that the IPO is leading by half of the year. For example, the calendar year IPO for 2000 is correlated to the 2000/01 thermal year variables from the respective ice cores. The higher correlations between the calendar year IPO and thermal year ice core variables are likely due in part to the intrinsic lag time between oceanic and atmospheric processes in the climate system.

The five PCs were used to perform stepwise linear regressions onto annual and seasonal IPO indices for the 1900–96 calibration period. For the annual IPO, factors 1, 2, and 5 were significant regressors in the model. Regression analysis was also performed for the pre- and post-1950 calibration periods to test the robustness of each model. PCR analysis was also performed for subsets of the ice core records, which demonstrated that the best-performing regression model included all four ice core sites. The calibration period made little difference to the models. Figure S4 shows the correlation coefficients between the observed IPO and the ice core–derived IPO for four different calibration periods. The linear regression equation for the ice core–derived IPO used in this study is

$$\text{IPO(Jan–Dec)}_{\text{Pred}} = (-0.128 \times \text{PC1}) + (0.167 \times \text{PC2})$$
$$+ (-0.248 \times \text{PC5}) + (-0.251).$$

Uncertainty in the regression model was estimated using a bias-corrected and accelerated bootstrapping method of 10 000 random samples to determine the 95% confidence intervals for each regression coefficient and the root-mean-square error of the verification period ($\text{RMSE}_\nu = 0.470$ for 1854–1900).

3. Characteristics of the IPO reconstruction

The annually resolved IPO reconstruction to 1450 CE is shown in Fig. 2a and compared with the observational record (1854–2010 CE) in Fig. 2b. The regression model explains 24.6% of the variance ($R^2_{\text{ADJ}} = 0.246$) in the annual IPO record

and is statistically significant according to the analysis of variance ($F = 9.31$; $p < 0.001$). When the interannual variability is smoothed to decadal resolution, the regression model explains 50.3% of the variance ($R^2_{\text{ADJ}} = 0.503$). The unitless model bias, mean average error, and root-mean-square error over the observational period are 0.021, 0.417, and 0.528, respectively (Table S3). Although the annual and decadal variability are well captured, the model amplitude is less than the observed amplitude. This is likely due to local climatic conditions at each ice core site as well as post-depositional impacts on the preserved ice core records. The reduced amplitude has little impact on the following correlative, composite, and spectral analyses. Model skill statistics are shown in Table S3 and demonstrate that the choice of calibration period has little effect on the resulting model performance.

As shown in the linear regression equation, the ice core–derived model is a combination of PCs 1, 2, and 5. To examine the physical links between these PCs and the IPO, spatial correlation fields for surface air temperature and sea level pressure were determined for each PC (Fig. S5). PC2 and PC5 capture the observed IPO temperature patterns over the Pacific basin. For instance, PC5 captures the horseshoe pattern along the west coast of North America, while PC2 captures the eastern equatorial tongue. PC2 also exhibits the sea level pressure dipole between the eastern and western Pacific, which is also influenced by the IPO. Although PC1 does not show much IPO coherence in the Pacific Basin, the temperature patterns in the Indian Ocean are reflective of the IPO pattern. Thus, the temperature and pressure variance captured by PCs 1, 2, and 5 combine to reveal a cohesive IPO pattern.

Throughout the last ~550 years, the reconstructed IPO index exhibits significant (>95%) periodicity in the ~30–70-yr multidecadal range, the decadal (~10 yr) range, and the higher-frequency 2–4-yr range (Figs. 3a,b). The multidecadal variability is typical of these large-scale climate patterns like the IPO and PDO. The higher-frequency variability is also typical as it falls in the time scale of ENSO. Wavelet analysis indicates that both the high-frequency and multidecadal variability persist for much of the last 550 years except during the ~1600–1750 CE period when multidecadal variability is relatively absent (Figs. 3c,d). Previous IPO/PDO reconstructions have shown that the 50–70-yr periodicity is most prevalent after 1850 CE and nearly absent during the Little Ice Age (Biondi et al. 2001; D'Arrigo et al. 2001; MacDonald and Case 2005; Shen et al. 2006). Similar results are found here, as the ~1800 CE peak in the 30–70-yr range in Fig. 3d is dominated by the 30–50-yr periodicity (Fig. 3c). During the 1600–1750 CE period, when multidecadal variability diminishes, centennial-scale variability appears more active (Fig. 3c), perhaps suggesting lower-frequency solar or internal variability. However, the IPO reconstruction is currently not long enough to determine centennial variations with confidence. Variability in the ENSO (2–8 yr) range appears more amplified during the 1650–1900 CE period (Fig. 3d), which suggests that higher-frequency events like El Niño and La Niña were more influential on the climate at the ice core sites during this time than, for example, in the twentieth century.
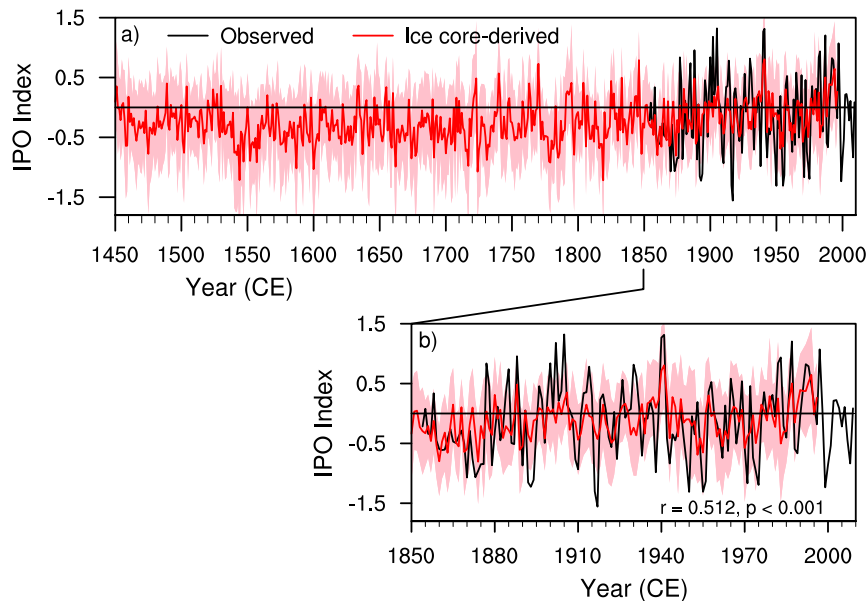
FIG. 2. The ice core–derived IPO reconstruction (red) with annual resolution to 1450 CE. The observed IPO from Henley et al. (2015) is shown in black. Results are shown for (a) the full record and (b) the instrumental period (1854–2010 CE). Shading represents estimated uncertainty in the reconstruction.

Multidecadal variability in the IPO reconstruction peaks ~1800 CE. However, outside of this peak, the wavelet characteristics are very similar to those from Shen et al. (2006), whose PDO reconstruction is based on historical drought/flood indices from eastern China. Shi et al. (2019) attribute the multidecadal variability in Asian summer rainfall to fluctuations in the Atlantic multidecadal oscillation (AMO). South American precipitation is influenced by the AMO (Apaéstegui et al. 2014), which likely influences the Quelccaya ice core site, as it receives much of its moisture from the tropical Atlantic (Thompson et al. 2013). During the 1600–1700 CE period, when multidecadal variability in the IPO reconstruction was weak, accumulation at Quelccaya was persistently above average (Thompson et al. 2013) due to the southward position of the ITCZ and $\delta^{18}O$ was below average. The AMO has also been shown to be related to, or even a driver of, Pacific climate variability (d'Orgeville and Peltier 2007; Zhang and Delworth 2007; Sun et al. 2017). Thus, further investigations are needed to tease out the Atlantic influence on the Pacific climate system.

a. Validation with observations

The reconstructed IPO index compares well with the observed IPO pattern among several climatic variables over the instrumental period (Fig. 4). Correlation fields between surface air temperature and both the observed and reconstructed IPO are quite similar, although the coefficients are somewhat muted for the reconstructed IPO compared to the observations. This is expected given the local climatic impacts at each ice core site and the post-depositional impacts on the preserved ice core records. Nevertheless, the positive correlations in the

eastern equatorial Pacific are apparent along with the negative correlation regions in the central North Pacific and off the east coast of Australia. Sea level pressure correlations are also similar between the reconstructed and observed IPO, as both display a pressure dipole between the western and eastern Pacific. Precipitation patterns are similar showing a positive band of correlation coefficients over the equatorial Pacific and negative correlations over the area of the SPCZ. Last, the relationship between the IPO and the Palmer Drought Severity Index (PDSI) shows negative correlation coefficients across eastern Asia and south through Indonesia and Australia. Positive correlations are evident over Eurasia and the Middle East. Both North and South America exhibit negative correlations to the north and positive correlations to the south. Each of these climate variables demonstrates the strong similarities between the observed and reconstructed IPO over the instrumental period.

b. Validation with paleo-proxy data assimilation products

Paleo-proxy data assimilation products combine multiproxy networks with climate models to produce gridded datasets of climate variables over the last millennium. PHYDA and LMR v2.0 and v2.1 are used to further validate the ice core–derived IPO reconstruction. These paleo-assimilation products are not independent due to considerable overlap among the individual proxy networks utilized. Similarly, these products are not entirely independent from the reconstructed IPO, as the oxygen isotope records from Quelccaya and Dasuopu are included in both assimilations. However, these assimilation products combine ~500 (LMR v2.1) and ~3000 (PHYDA, LMR v2.0) different paleo-proxy records, such that the overall impact of
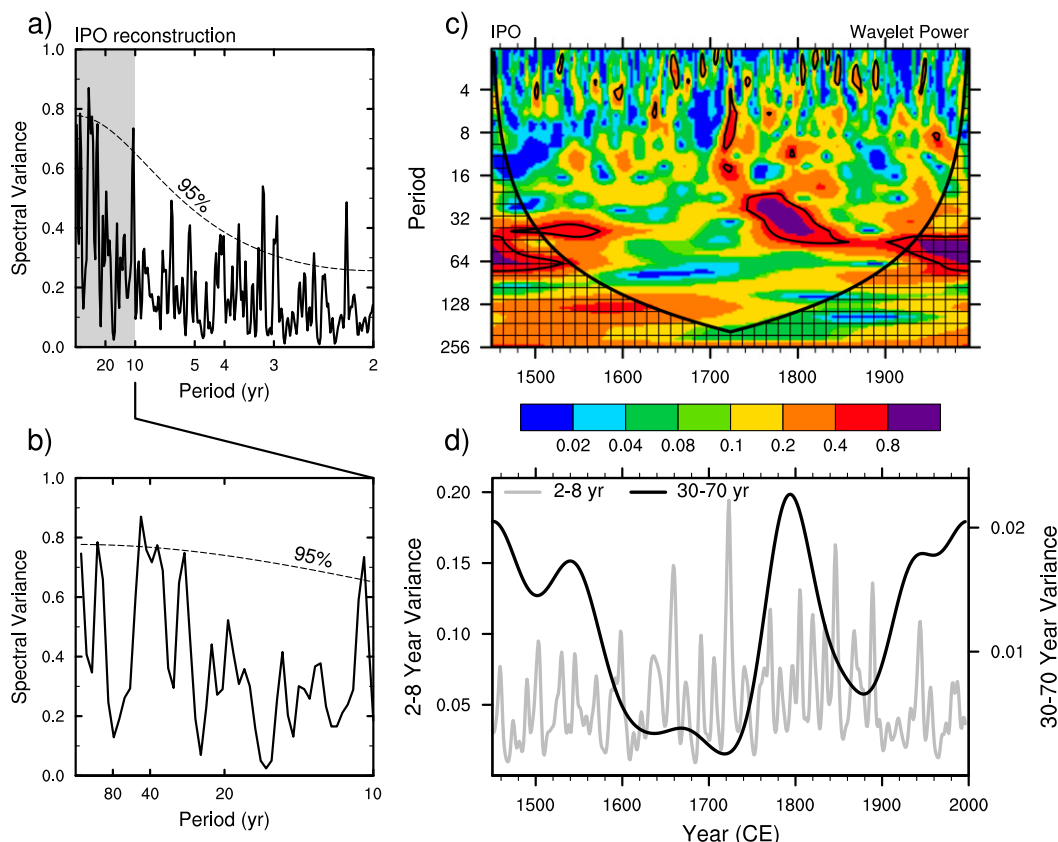
FIG. 3. (a) Spectral power of the ice core–derived IPO index and (b) an inset of the decadal-to-multidecadal power spectra; (c) wavelet analysis for the reconstructed IPO; black outlines represent 95% significance; (d) the average variance in the 2–8-yr (gray) and 30–70-yr (black) periods.

the Quelccaya and Dasuopu records should be minimal in each assimilation. Given the limited number of these comprehensive, global paleo-assimilation datasets that are currently available, the overlap with the individual ice core records from this study is unavoidable.

Composites of surface air temperature (SAT) and PDSI were created by averaging the anomalies for both positive and negative IPO events (±1.5 standard deviations) using the ice core–derived IPO reconstruction and then calculating the difference. The years used in the composites are listed in Table S4. The composites thereby represent the positive-minus-negative IPO signal in SAT and PDSI using each gridded paleo-assimilation dataset for the 1450–1996 CE period (Figs. 5a–c,e–g) and the observed IPO signal in SAT and PDSI for the 1948–2018 CE period (Figs. 5d,h). The SAT paleo-composites (Figs. 5a–c) strongly resemble the observed composite (Fig. 5d), especially in the eastern equatorial Pacific and along the west coast of North America. The observed negative anomalies in the central North Pacific and along the SPCZ are not captured as well by the paleo-assimilations. This may reflect the lack of paleo-proxy data from those regions. The PDSI composites from the paleo-assimilations (Figs. 5e–g) are also very similar to the observed composite (Fig. 5h). This analysis serves to validate the ice core–derived IPO index regarding both the climate signals recorded in

the ice cores and the time scales determined for the ice core records. Timescale accuracy is critical for all paleo-proxy data and achieving consistent accuracy among different proxy records is difficult. Thus, the fact that individual years chosen from the IPO reconstruction align with the individual years in the assimilations suggests that time scale errors are minimal.

Spatial correlation fields were also determined between the IPO reconstruction and the paleo-assimilations (Fig. S6) to analyze the relationships for all years and not just for the extreme years as determined for the composite analysis. These correlation fields for SAT and PDSI are like those observed in Fig. 4. Likewise, correlation coefficients were determined for each century to determine the temporal stationarity of the IPO signal (Figs. S7 and S8). Although the SAT and PDSI correlations are somewhat weaker in the seventeenth and nineteenth centuries, the relationship between the reconstructed IPO index and global climate is robust. Figures S7 and S8 only show the correlations between the IPO and PHYDA variables; however, the results were similar when using LMR v2.0 and v2.1 (not shown).

c. Comparison with previous reconstructions

Numerous reconstructions of Pacific climate variability have been created to investigate the multidecadal behavior of the
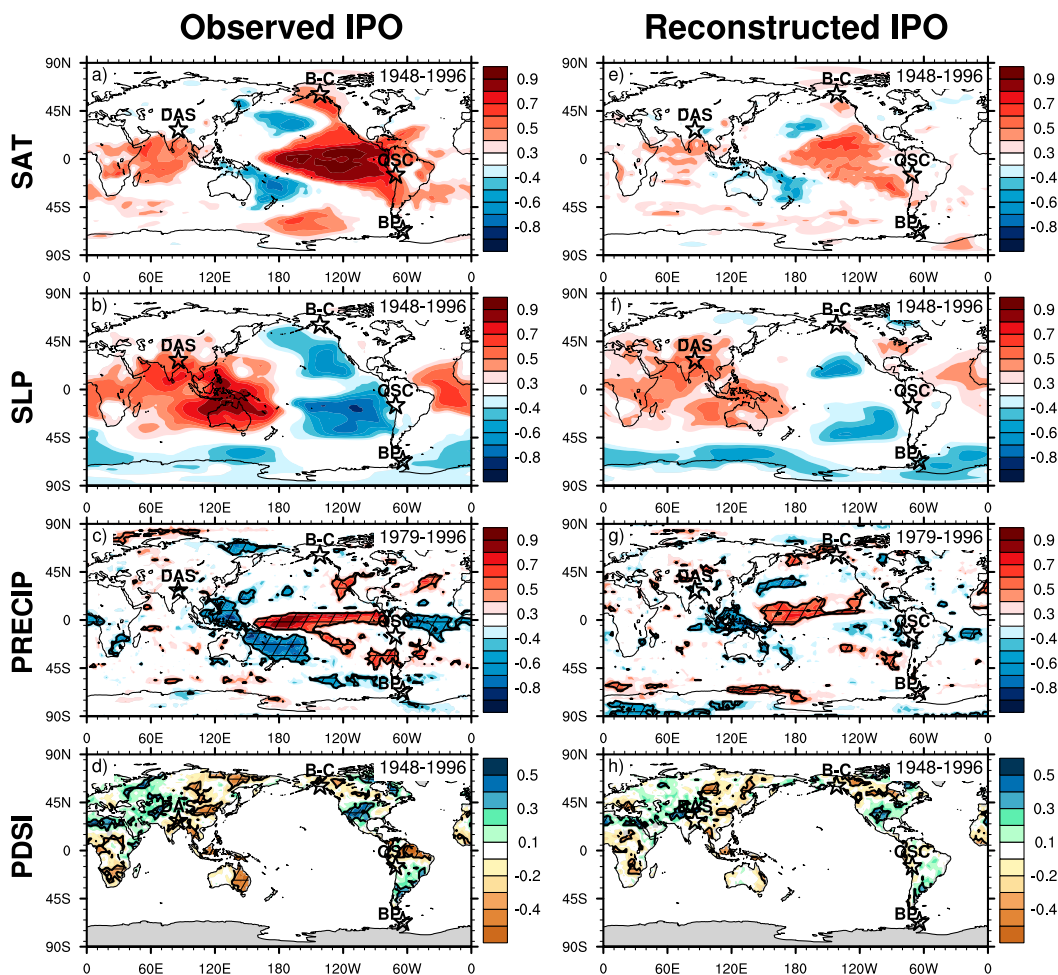
FIG. 4. Correlation coefficients between the (a)–(d) observed and (e)–(h) reconstructed IPO with (a),(e) surface air temperature and (b),(f) sea level pressure (1948–96) from the NCEP–NCAR (1996) reanalysis, (c),(g) precipitation (1979–96) from GPCP (2016), and (d),(h) PDSI (1948–96) from Dai (2017). Only significant (>95%) correlations are shaded in the (a),(e) surface air temperature and (b),(f) sea level pressure panels. Hatching in (c), (d), (g), and (h) represents the >95% significance level.

climate system. Many of these reconstructions focus on the climatic effects of the PDO or IPO on one limited area such as western North America or eastern Asia. Due in part to their limited regional coverage, there is little agreement among the 10 or so previous reconstructions of PDV (Wise 2015; Henley 2017). Nevertheless, we compare our ice core–derived IPO index with these reconstructions (Fig. 6). The LMRv2.0 dataset includes the tree ring records that were used to generate several of the other reconstructions shown in Fig. 6; hence, the PDO index derived from LMR contains some overlap with the other tree ring–derived reconstructions. PDO or IPO indices are not available from PHYDA as only air temperature (not SST) and PDSI are included in the assimilation. The reconstructions demonstrate good agreement over the twentieth century as expected since this contains the calibration period. Figure S9 indicates stronger agreement among the reconstructions over the twentieth and eighteenth centuries. Correlations between the IPO from this study and previous

reconstructions are stronger after 1750 CE (Table S5). There is also agreement in the early part of the records (pre-1600 CE) as several records show a pronounced positive IPO/PDO phase. The timing of this period varies somewhat; thus, the correlations are weaker before 1750 CE (Table S5). The IPO index from this study and the PDO index from Shen et al. (2006), for instance, show the positive phase ending a decade or two earlier than the other reconstructions. The composite record of the seven previous paleo-proxy reconstructions (Fig. 6) shows good coherence with the ice core–derived IPO. Although the IPO constructed in this study shows lower magnitude events compared to observations (Fig. 2b), both the composite and this IPO index show relatively higher-amplitude events before 1550 CE and after 1900 CE and lower-amplitude fluctuations between 1550 and 1900 CE. These lower-amplitude fluctuations are predominantly in the negative IPO phase. The ice core–derived IPO reconstruction, which uses four well-dated, spatially diverse records, captures the main features of the

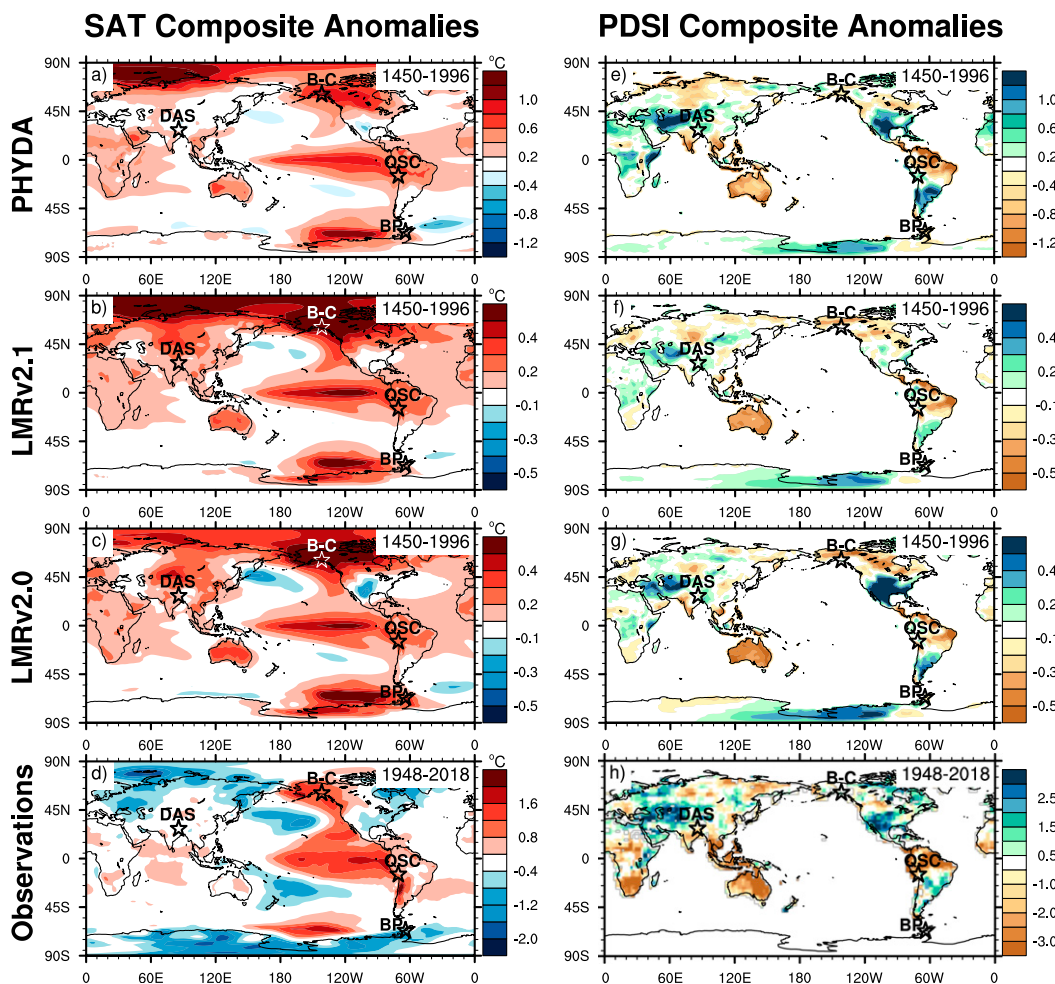## SAT Composite Anomalies   PDSI Composite Anomalies

FIG. 5. Composite (a)–(d) temperature and (e)–(h) PDSI anomalies for positive minus negative IPO events from paleo-proxy data assimilation products: (a),(e) PHYDA, (b),(f) LMR v2.1, and (c),(g) LMR v2.0 for the 1450–1996 CE period. (d),(h) The observed composite anomalies for the 1948–2018 CE period. Reconstructed IPO events ± 1.5 standard deviations from the mean are included in the composites (Table S2), and the 10 highest minus 10 lowest observed IPO events (Table S2) are included in (d) and (h).

composite record, which incorporates numerous proxy records from around the globe.

4. IPO and external forcing interactions during the Little Ice Age

The ice core–derived IPO reconstruction indicates that a negative IPO state dominated much of the Little Ice Age (LIA) (Fig. 6) in agreement with several older reconstructions, exhibiting an average negative phase during the eighteenth century (Fig. S9). This characterization of the LIA arises from the contribution of the different proxy indicators preserved in four ice core records upon which the IPO reconstruction is based. The Quelccaya accumulation record shows a sharp transition from wetter to drier conditions at ~1700 CE due to the northward migration of the ITCZ in the latter half of the LIA. This suggests a shift from an El Niño–like state to a La

Niña–like state at ~1700 CE. However, depleted (more negative) $\delta^{18}O$ values throughout much of the LIA reflect cooler conditions in the eastern equatorial Pacific (Thompson et al. 2013) and hence, a more La Niña–like state. The Bona–Churchill core shows enriched $\delta^{18}O$ during the LIA likely due to a weaker Aleutian low (Porter et al. 2019), which generally corresponds to negative PDO/IPO conditions. After 1850 CE, the IPO reconstruction remains in a predominantly positive phase, consistent with the Dasuopu records of increasing $\delta^{18}O$ and dust concentrations and decreasing accumulation over much of the twentieth century. These conditions suggest a warming trend and a weakening monsoon (Thompson et al. 2000, 2006) and thereby resemble a more El Niño–like state during the current warm period.

A prolonged negative IPO, as observed in the IPO reconstruction during the LIA, would generally include more frequent La Niña events (Verdon and Franks 2006; Sun and
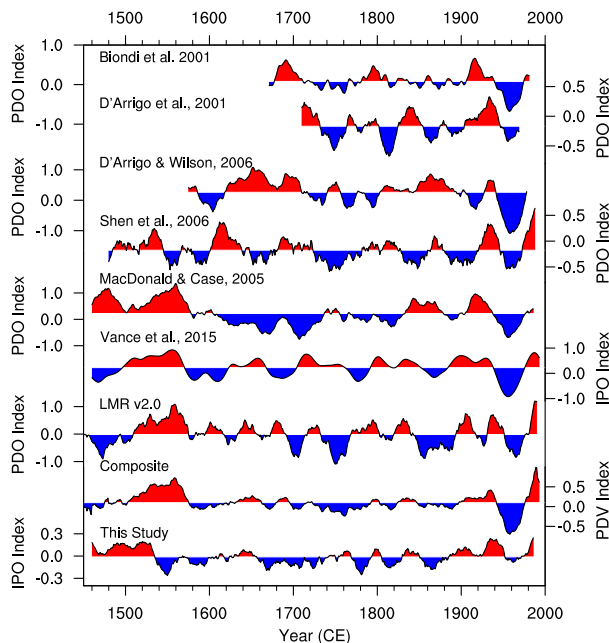
FIG. 6. Time series of seven PDO and IPO reconstructions and a simple Pacific decadal variability (PDV) composite of these seven series compared with the ice core–derived IPO from this study. Data are shown as 21-yr running means.
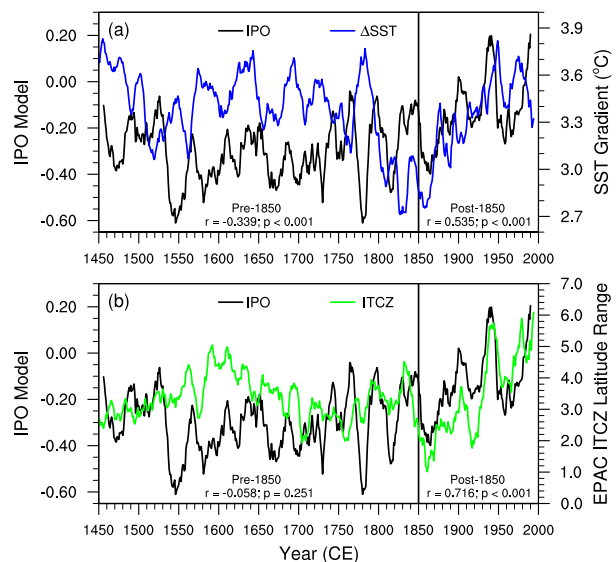

FIG. 7. Time series of the reconstructed IPO index (black) and (a) the equatorial Pacific SST gradient from PHYDA (blue) and (b) the eastern Pacific ITCZ latitudinal range (green) from PHYDA. Data are shown as 13-yr running means. The line at 1850 CE marks the approximate end of the Little Ice Age.

Okumura 2020); however, numerous studies suggest that the LIA climate was more El Niño–like (Cobb et al. 2003; Mann et al. 2005, 2009). Many of the proxies that indicate an enhanced El Niño–like state during the LIA capture a decreased equatorial ocean temperature gradient between the western and eastern Pacific and/or a southward shift in the ITCZ. However, hydrological records have indicated that an enhanced Walker circulation is common with La Niña events and, rather than a pronounced southward shift in the ITCZ, a contraction of the latitudinal range of the ITCZ around the equator (Yan et al. 2015; Griffiths et al. 2016). In further contrast, Henke et al. (2017) and Zhou et al. (2020) have suggested that there is little difference in the mean climate state of the Pacific Ocean among the Medieval Climate Anomaly, the LIA, and current warm period. Future work combining paleo-proxy records and climate modeling is required to better understand tropical Pacific climate dynamics throughout Earth's climate history.

From the PHYDA paleo-proxy assimilation (Steiger et al. 2018), the Pacific SST gradient and latitudinal range of the eastern Pacific ITCZ are compared with the IPO reconstruction (Fig. 7). The latitudinal range was determined by the difference between the boreal summer (JJA) and winter (DJF) latitudinal positions of the ITCZ, and the eastern Pacific region (170°–260°E) was chosen due to PHYDA's stronger skill in reconstructing the ITCZ position in that region than in the western Pacific region (Steiger et al. 2018). During the current warm period (post-1850 CE), the IPO is positively related to the SST gradient and ITCZ range, such that a positive IPO is related to a stronger thermal gradient and larger range of the

ITCZ. Each variable is dominated by an increasing trend after 1850 CE, which likely influences the correlation coefficients. As the trend is steepest after 1850 CE, detrending each variable over the full 1450–1996 CE period makes little difference to the correlation coefficients. Detrending each variable over the post-1850 period, however, reduces the correlation coefficients determined between the IPO reconstruction and the SST gradient to $r = 0.153$ ($p = 0.070$) and the ITCZ range to $r = 0.568$ ($p < 0.001$). Thus, in the current warm period, there is little connection between the IPO reconstruction and the tropical Pacific SST gradient; however, the IPO reconstruction is strongly correlated with the latitudinal range of the ITCZ.

The latitudinal range of the ITCZ determined from PHYDA also supports an expansion of the eastern Pacific ITCZ in the current warm period and a contraction during the LIA. Prior to 1850 CE, relationships between the IPO and both SST gradient and ITCZ range weaken considerably and even change sign (Fig. 7), such that a positive IPO coincides with a weakened SST gradient and reduced latitudinal range in the ITCZ. According to the wavelet analysis (Fig. 3d), the ice core–derived IPO reconstruction exhibits little multidecadal variability from 1600 to 1750 CE, when subdecadal and centennial variability dominated. The relationship between the IPO and the ITCZ range is virtually absent during the LIA. This suggests that the state of the IPO had little impact on the ITCZ contraction, both of which were possibly forced by external factors such as reduced solar forcing and/or enhanced volcanic forcing.

The response of tropical Pacific climate variability to volcanic and solar forcing has been studied extensively; however, there is still considerable uncertainty associated with these responses. While recent work by Dee et al. (2020) shows little
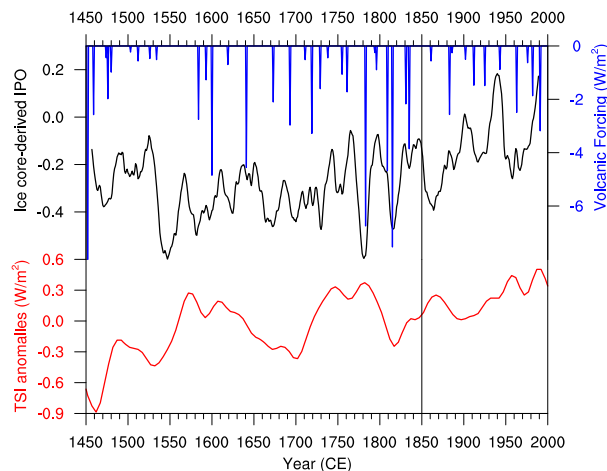
FIG. 8. The reconstructed IPO index with volcanic forcing (W m^{-2}; blue) from Gao et al. (2008) and total solar irradiance (TSI; red) from Steinhilber et al. (2009) back to 1450 CE. TSI is given as anomalies to the mean solar irradiance of 1364.5 W m^{-2} for the 1450–2000 CE period. The line at 1850 CE marks the approximate end of the Little Ice Age.

influence of volcanic forcing on ENSO, numerous other studies suggest that El Niño events can be triggered by explosive volcanic eruptions (Adams et al. 2003; Mann et al. 2005; Emile-Geay et al. 2008; Lim et al. 2016; Maher et al. 2015; Stevenson et al. 2016). Some studies suggest that after an initial El Niño–like response to an eruption, a persistent La Niña may develop up to 3+ years post-eruption (Maher et al. 2015; Pausata et al. 2015), which in combination with reduced solar irradiance can influence the long-term state of the Pacific by initiating a negative PDO phase (Wang et al. 2012). Comparing the ice core–derived IPO index with volcanic activity over the last 550 years does not show a clear response to volcanic forcing (Fig. 8); however, some interesting features do appear. Volcanic activity is greater prior to 1850 CE during the LIA, and the IPO is generally more negative during this time relative to the current warm period (Fig. 8). Also, two of the peaks in volcanic forcing occur around 1783 CE (Laki) and 1815 CE (Tambora). These two major eruptions also coincide with two of the three most extreme, negative phases of the IPO. There is, however, an extremely low IPO event ~1550 CE, which shows no coincidental timing with volcanic activity. After 1850 CE, volcanic activity begins to decline. Although solar irradiance increases steadily throughout the 1450–2000 CE period, the IPO only exhibits a strong positive trend after 1850 CE. Further investigation with climate models is needed to elucidate the role of external forcings on tropical Pacific climate during the LIA.

It is also difficult to determine how the IPO may be affected by increased anthropogenic forcing. Some studies have suggested that both greenhouse gases and anthropogenic aerosols influence PDV (Dong et al. 2014; Smith et al. 2016), but the responses are again mixed. Dong et al. (2014) attribute the positive trend in PDV to increased tropical warming due to greenhouse gases and cooling over the central North Pacific

due to anthropogenic aerosols. Smith et al. (2016) suggest that increased anthropogenic aerosol emissions over China and decreased aerosol emissions over North America initiate a negative PDO by weakening the Aleutian low. Likewise, the SST signature of El Niño events has been evolving from the canonical eastern Pacific El Niño to the central Pacific El Niño, as coral records indicate the increased frequency of central Pacific events in the twentieth century (Freund et al. 2019). Thus, the response of tropical Pacific climate variability to a warming world requires further investigation.

5. Conclusions

Using an assemblage of ice cores collected around the Pacific basin, one of the first basinwide histories of Pacific climate variability has been created. This ice core–derived IPO index incorporates ice core records from South America, the Himalaya, the Antarctic Peninsula, and northwestern North America. The reconstructed IPO is annually resolved and dates to 1450 CE. Comparisons between the observed and reconstructed IPO indices and their relationships with observed climatic variables show a strong resemblance over the instrumental period. Paleo-proxy assimilation datasets such as PHYDA and LMR are similarly used to validate the IPO reconstruction further back in time. The IPO reconstruction demonstrates a strong and temporally stationary IPO signal for the past 550 years. The agreement between the IPO reconstruction and the assimilation products validates the ice core–derived IPO reconstruction and alleviates concerns regarding possible time scale errors. Thus, this ice core–derived IPO reconstruction, which uses four well-dated, spatially diverse sites, captures the main features of Pacific climate variability as demonstrated by the PHYDA and LMR datasets, which incorporate numerous proxy records from around the globe. The comparison between the ice core–derived IPO index and previous reconstructions demonstrates some similarities, although the geographical extent represented by many previous reconstructions is limited.

The reconstructed IPO index suggests that the LIA was primarily defined by a negative IPO phase and hence more La Niña–like conditions. The mean ENSO state during the LIA remains uncertain; however, the reconstructed IPO reveals some interesting dynamics with the ITCZ. In the current warm period, the latitudinal range of the ITCZ is positively related to the IPO such that a positive IPO increases the seasonal range of the ITCZ. This relationship is not stationary and is nearly absent prior to 1850 CE and throughout the LIA. External forcing from volcanoes and reduced solar irradiance may have influenced the ITCZ shifts and/or the climate at the ice core sites included in the IPO reconstruction. Future work is needed to explore these dynamics more thoroughly. Further investigations of the interactive effects between the multidecadal background state of the Pacific Ocean and individual ENSO events using global climate model simulations are in progress. These simulations will help identify physical mechanisms influencing the climate at these ice core sites and clarify how signals of those mechanisms are preserved in the ice core records.

REFERENCES

Adams, J. B., M. E. Mann, and C. M. Ammann, 2003: Proxy evidence for an El Niño-like response to volcanic forcing. *Nature*, **426**, 274–278, https://doi.org/10.1038/nature02101.

Adler, R. F., and Coauthors, 2018: The Global Precipitation Climatology Project (GPCP) monthly analysis (new version 2.3) and a review of 2017 global precipitation. *Atmosphere*, **9**, 138, https://doi.org/10.3390/atmos9040138.

Anderson, D. M., R. Tardif, K. Horlick, M. P. Erb, G. J. Hakim, D. Noone, W. A. Perkins, and E. Steig, 2019: Additions to the Last Millennium Reanalysis multi-proxy database. *Data Sci. J.*, **18**, 2, https://doi.org/10.5334/dsj-2019-002.

Andreoli, E. V., and M. T. Kayano, 2005: ENSO-related rainfall anomalies in South America and associated circulation features during warm and cold Pacific decadal oscillation regimes. *Int. J. Climatol.*, **25**, 2017–2030, https://doi.org/10.1002/joc.1222.

Apaéstegui, J., and Coauthors, 2014: Hydroclimate variability of the northwestern Amazon Basin near the Andean foothills of Peru related to the South American monsoon system during the last 1600 years. *Climate Past*, **10**, 1967–1981, https://doi.org/10.5194/cp-10-1967-2014.

Biondi, F., A. Gershunov, and D. R. Cayan, 2001: North Pacific decadal climate variability since 1661. *J. Climate*, **14**, 5–10, https://doi.org/10.1175/1520-0442(2001)014<0005:NPDCVS>2.0.CO;2.

Bond, N. A., J. E. Overland, M. Spillane, and P. Stabeno, 2003: Recent shifts in the state of the North Pacific. *Geophys. Res. Lett.*, **30**, 2183, https://doi.org/10.1029/2003GL018597.

Buckley, B. M., C. C. Ummenhofer, R. D. D'Arrigo, K. G. Hansen, L. H. Truong, C. N. Le, and D. K. Stahle, 2019: Interdecadal Pacific oscillation reconstructed from trans-Pacific tree rings: 1350–2004 CE. *Climate Dyn.*, **53**, 3181–3196, https://doi.org/10.1007/s00382-019-04694-4.

Chen, B., S. R. Smith, and D. H. Bromwich, 1996: Evolution of the tropospheric split jet over the South Pacific Ocean during the 1986–89 ENSO cycle. *Mon. Wea. Rev.*, **124**, 1711–1731, https://doi.org/10.1175/1520-0493(1996)124<1711:EOTTSJ>2.0.CO;2.

Clem, K. R., and R. L. Fogt, 2013: Varying roles of ENSO and SAM on the Antarctic Peninsula climate in austral spring. *J. Geophys. Res. Atmos.*, **118**, 11 481–11 492, https://doi.org/10.1002/jgrd.50860.

——, A. Orr, and J. O. Pope, 2018: The springtime influence of natural tropical Pacific variability on the surface climate of the Ross Ice Shelf, West Antarctica: Implications for ice shelf thinning. *Sci. Rep.*, **8**, 11983, https://doi.org/10.1038/s41598-018-30496-5.

Cobb, K. M., C. D. Charles, H. Cheng, and R. L. Edwards, 2003: El Niño/Southern Oscillation and tropical Pacific climate during the last millennium. *Nature*, **424**, 271–276, https://doi.org/10.1038/nature01779.

Dai, A., 2017: Dai Global Palmer Drought Severity Index (PDSI). National Center for Atmospheric Research, Computational and Information Systems Laboratory, accessed 4 February 2020, https://doi.org/10.5065/D6QF8R93.

——, K. E. Trenberth, and T. Qian, 2004: A global data set of Palmer Drought Severity Index for 1870–2002: Relationship with soil moisture and effects of surface warming. *J. Hydrometeor.*, **5**, 1117–1130, https://doi.org/10.1175/JHM-386.1.

D'Arrigo, R., and R. Wilson, 2006: On the Asian expression of the PDO. *Int. J. Climatol.*, **26**, 1607–1617, https://doi.org/10.1002/joc.1326.

——, R. Villalba, and G. Wiles, 2001: Tree-ring estimates of Pacific decadal climate variability. *Climate Dyn.*, **18**, 219–224, https://doi.org/10.1007/s003820100177.

Dee, S. G., K. M. Cobb, J. Emile-Geay, T. R. Ault, R. L. Edwards, H. Cheng, and C. Charles, 2020: No consistent ENSO response to volcanic forcing over the last millennium. *Science*, **367**, 1477–1481, https://doi.org/10.1126/science.aax2000.

Deser, C., A. S. Phillips, and J. W. Hurrell, 2004: Pacific interdecadal climate variability: Linkages between the tropics and the North Pacific during boreal winter since 1900. *J. Climate*, **17**, 3109–3124, https://doi.org/10.1175/1520-0442(2004)017<3109:PICVLB>2.0.CO;2.

Di Lorenzo, E., G. Liguori, N. Schneider, J. C. Furtado, B. T. Anderson, and M. A. Alexander, 2015: ENSO and meridional modes: A null hypothesis for Pacific climate variability. *Geophys. Res. Lett.*, **42**, 9440–9448, https://doi.org/10.1002/2015GL066281.

Dong, B., and A. Dai, 2015: The influence of the interdecadal Pacific oscillation on temperature and precipitation over the globe. *Climate Dyn.*, **45**, 2667–2681, https://doi.org/10.1007/s00382-015-2500-x.

——, ——, M. Vuille, and O. E. Timm, 2018: Asymmetric modulation of ENSO teleconnections by the interdecadal Pacific oscillation. *J. Climate*, **31**, 7337–7361, https://doi.org/10.1175/JCLI-D-17-0663.1.

Dong, L., T. Zhou, and X. Chen, 2014: Changes of Pacific decadal variability in the twentieth century driven by internal variability, greenhouse gases, and aerosols. *Geophys. Res. Lett.*, **41**, 8570–8577, https://doi.org/10.1002/2014GL062269.

d'Orgeville, M., and W. R. Peltier, 2007: On the Pacific decadal oscillation and the Atlantic multidecadal oscillation: Might they be related? *Geophys. Res. Lett.*, **34**, L23705, https://doi.org/10.1029/2007GL031584.

Emile-Geay, J., R. Seager, M. A. Cane, E. R. Cook, and G. H. Haug, 2008: Volcanoes and ENSO over the past millennium. *J. Climate*, **21**, 3134–3148, https://doi.org/10.1175/2007JCLI1884.1.

Folland, C. K., D. E. Parker, A. Colman, and R. Washington, 1999: Large scale modes of ocean surface temperatures since the late nineteenth century. *Beyond El Niño: Decadal and Interdecadal Climate Variability*, A. Navarra, Ed., Springer, 73–102, https://doi.org/10.1007/978-3-642-58369-8.

——, J. A. Renwick, M. J. Salinger, and A. B. Mullan, 2002: Relative influences of the interdecadal Pacific oscillation and ENSO on the South Pacific convergence zone. *Geophys. Res. Lett.*, **29**, 1643, https://doi.org/10.1029/2001GL014201.

Freund, M. B., B. J. Henley, D. J. Karoly, H. V. McGregor, N. J. Abram, and D. Dommenget, 2019: Higher frequency of

Central Pacific El Niño events in recent decades relative to past centuries. *Nat. Geosci.*, **12**, 450–455, https://doi.org/10.1038/s41561-019-0353-3.

Gao, C., A. Robock, and C. Ammann, 2008: Volcanic forcing of climate over the past 1500 years: An improved ice core–based index for climate models. *J. Geophys. Res.*, **113**, D23111, https://doi.org/10.1029/2008JD010239.

Gedalof, Z., and D. J. Smith, 2001: Interdecadal climate variability and regime-scale shifts in Pacific North America. *Geophys. Res. Lett.*, **28**, 1515–1518, https://doi.org/10.1029/2000GL011779.

Gershunov, A., and T. P. Barnett, 1998: Interdecadal modulation of ENSO teleconnections. *Bull. Amer. Meteor. Soc.*, **79**, 2715–2725, https://doi.org/10.1175/1520-0477(1998)079<2715:IMOET>2.0.CO;2.

Goodwin, B. G., E. Mosley-Thompson, A. B. Wilson, S. E. Porter, and M. R. Sierra-Hernández, 2016: Accumulation variability in the Antarctic Peninsula: The role of large-scale atmospheric oscillations and their interactions. *J. Climate*, **29**, 2579–2596, https://doi.org/10.1175/JCLI-D-15-0354.1.

GPCP, 2016: GPCP version 2.3 combined precipitation data set. NOAA/Earth Systems Research Laboratory/Physical Sciences Laboratory, accessed 22 November 2019, https://psl.noaa.gov/data/gridded/data.gpcp.html.

Griffiths, M. L., and Coauthors, 2016: Western Pacific hydroclimate linked to global climate variability over the past two millennia. *Nat. Commun.*, **7**, 11719, https://doi.org/10.1038/ncomms11719.

Henke, L. M. K., F. H. Lambert, and D. J. Charman, 2017: Was the Little Ice Age more or less El Niño-like than the Medieval Climate Anomaly? Evidence from hydrological and temperature proxy data. *Climate Past*, **13**, 267–301, https://doi.org/10.5194/cp-13-267-2017.

Henley, B. J., 2015: TPI (IPO) Tripole Index for the Interdecadal Pacific Oscillation (unfiltered from NOAA ERSST V5). NOAA/Earth System Research Laboratory/Physical Sciences Laboratory, accessed 25 June 2018, https://psl.noaa.gov/data/timeseries/IPOTPI/.

——, 2017: Pacific decadal climate variability: Indices, patterns, and tropical–extratropical interactions. *Global Planet. Change*, **155**, 42–55, https://doi.org/10.1016/j.gloplacha.2017.06.004.

——, and A. D. King, 2017: Trajectories toward the 1.5°C Paris target: Modulation by the interdecadal Pacific oscillation. *Geophys. Res. Lett.*, **44**, 4256–4262, https://doi.org/10.1002/2017GL073480.

——, J. Gergis, D. J. Karoly, S. Power, J. Kennedy, and C. K. Folland, 2015: A tripole index for the interdecadal Pacific oscillation. *Climate Dyn.*, **45**, 3077–3090, https://doi.org/10.1007/s00382-015-2525-1.

Hu, Z.-Z., and B. Huang, 2009: Interferential impact of ENSO and PDO on dry and wet conditions in the U.S. Great Plains. *J. Climate*, **22**, 6047–6065, https://doi.org/10.1175/2009JCLI2798.1.

Kalnay, E., and Coauthors, 1996: The NCEP/NCAR 40-Year Reanalysis Project. *Bull. Amer. Meteor. Soc.*, **77**, 437–472, https://doi.org/10.1175/1520-0477(1996)077<0437:TNYRP>2.0.CO;2.

Kosaka, Y., and S.-P. Xie, 2016: The tropical Pacific as a key pacemaker of the variable rates of global warming. *Nat. Geosci.*, **9**, 669–673, https://doi.org/10.1038/ngeo2770.

Krishnan, R., and M. Sugi, 2003: Pacific decadal oscillation and variability of the Indian summer monsoon rainfall. *Climate Dyn.*, **21**, 233–242, https://doi.org/10.1007/s00382-003-0330-8.

Kumar, K. K., B. Rajagopalan, M. Hoerling, G. Bates, and M. Cane, 2006: Unraveling the mystery of Indian monsoon failure during El Niño. *Science*, **314**, 115–119, https://doi.org/10.1126/science.1131152.

Lim, H.-G., S.-W. Yeh, J.-S. Kug, Y.-G. Park, J.-H. Park, R. Park, and C.-K. Song, 2016: Threshold of the volcanic forcing that leads the El Niño-like warming in the last millennium: Results from the ERIK simulation. *Climate Dyn.*, **46**, 3725–3736, https://doi.org/10.1007/s00382-015-2799-3.

Linsley, B. K., P. Zhang, A. Kaplan, S. S. Howe, and G. M. Wellington, 2008: Interdecadal–decadal climate variability from multicoral oxygen isotope records in the South Pacific Convergence Zone region since 1650 A.D. *Paleoceanography*, **23**, PA2219, https://doi.org/10.1029/2007PA001539.

LMR, 2019: Last Millennium Reanalysis (LMR) Project Global Climate Reconstructions versions 2 and 2.1. National Centers for Environmental Information, accessed 3 January 2020, https://www.ncdc.noaa.gov/paleo-search/study/27850.

MacDonald, G. M., and R. A. Case, 2005: Variations in the Pacific decadal oscillation over the past millennium. *Geophys. Res. Lett.*, **32**, L08703, https://doi.org/10.1029/2005GL022478.

Maher, N., S. McGregor, M. H. England, and A. Sen Gupta, 2015: Effects of volcanism on tropical variability. *Geophys. Res. Lett.*, **42**, 6024–6033, https://doi.org/10.1002/2015GL064751.

Mann, M. E., R. S. Bradley, and M. K. Hughes, 1998: Global-scale temperature patterns and climate forcing over the past six centuries. *Nature*, **392**, 779–787, https://doi.org/10.1038/33859.

——, M. A. Cane, S. E. Zebiak, and A. Clement, 2005: Volcanic and solar forcing of the tropical Pacific over the past 1000 years. *J. Climate*, **18**, 447–456, https://doi.org/10.1175/JCLI-3276.1.

——, Z. Zhang, M. K. Hughes, R. S. Bradley, S. K. Miller, S. Rutherford, and F. Ni, 2008: Proxy-based reconstructions of hemispheric and global surface temperature variations over the past two millennia. *Proc. Natl. Acad. Sci. USA*, **105**, 13 252–13 257, https://doi.org/10.1073/pnas.0805721105.

——, and Coauthors, 2009: Global signatures and dynamical origins of the Little Ice Age and Medieval Climate Anomaly. *Science*, **326**, 1256–1260, https://doi.org/10.1126/science.1177303.

Mantua, N. J., S. R. Hare, Y. Zhang, J. M. Wallace, and R. C. Francis, 1997: A Pacific interdecadal climate oscillation with impacts on salmon production. *Bull. Amer. Meteor. Soc.*, **78**, 1069–1079, https://doi.org/10.1175/1520-0477(1997)078<1069:APICOW>2.0.CO;2.

Meehl, G. A., and A. Hu, 2006: Megadroughts in the Indian monsoon region and southwest North America and a mechanism for associated multidecadal Pacific sea surface temperature anomalies. *J. Climate*, **19**, 1605–1623, https://doi.org/10.1175/JCLI3675.1.

——, ——, J. M. Arblaster, J. Fasullo, and K. E. Trenberth, 2013: Externally forced and internally generated decadal climate variability associated with the interdecadal Pacific oscillation. *J. Climate*, **26**, 7298–7310, https://doi.org/10.1175/JCLI-D-12-00548.1.

——, J. M. Arblaster, C. M. Bitz, C. T. Y. Chung, and H. Teng, 2016: Antarctic sea ice expansion between 2000 and 2014 driven by tropical Pacific decadal climate variability. *Nat. Geosci.*, **9**, 590–595, https://doi.org/10.1038/ngeo2751.

Minobe, S., 1997: A 50–70 year climatic oscillation over the North Pacific and North America. *Geophys. Res. Lett.*, **24**, 683–686, https://doi.org/10.1029/97GL00504.

NCEP–NCAR, 1996: NCEP/NCAR reanalysis monthly means and other derived variables (updated monthly). NOAA/Earth Systems Research Laboratory/Physical Sciences Laboratory,

accessed 22 November 2019, https://psl.noaa.gov/data/gridded/data.ncep.reanalysis.derived.html.

Otto-Bliesner, B. L., and Coauthors, 2016: Climate variability and change since 850 CE: An ensemble approach with the Community Earth System Model. *Bull. Amer. Meteor. Soc.*, **97**, 735–754, https://doi.org/10.1175/BAMS-D-14-00233.1.

Overland, J. E., J. M. Adams, and N. A. Bond, 1999: Decadal variability of the Aleutian low and its relation to high-latitude circulation. *J. Climate*, **12**, 1542–1548, https://doi.org/10.1175/1520-0442(1999)012<1542:DVOTAL>2.0.CO;2.

PAGES 2k Consortium, 2017: A global multiproxy database for temperature reconstructions of the Common Era. *Sci. Data*, **4**, 170088, https://doi.org/10.1038/sdata.2017.88.

Pausata, F. S. R., L. Chafik, R. Caballero, and D. S. Battisti, 2015: Impacts of high-latitude volcanic eruptions on ENSO and AMOC. *Proc. Natl. Acad. Sci. USA*, **112**, 13 784–13 788, https://doi.org/10.1073/pnas.1509153112.

PHYDA, 2018: Paleo Hydrodynamics Data Assimilation product (PHYDA). Zenodo, accessed 1 September 2019, https://doi.org/10.5281/zenodo.1198817.

Porter, S. E., E. Mosley-Thompson, and L. G. Thompson, 2019: Ice core δ^{18}O record linked to western Arctic sea ice variability. *J. Geophys. Res. Atmos.*, **124**, 10 784–10 801, https://doi.org/10.1029/2019JD031023.

Power, S., T. Casey, C. Folland, A. Colman, and V. Mehta, 1999: Interdecadal modulation of the impact of ENSO on Australia. *Climate Dyn.*, **15**, 319–324, https://doi.org/10.1007/s003820050284.

Ropelewski, C. F., and M. S. Halpert, 1987: Global and regional scale precipitation patterns associated with the El Niño/Southern Oscillation. *Mon. Wea. Rev.*, **115**, 1606–1626, https://doi.org/10.1175/1520-0493(1987)115<1606:GARSPP>2.0.CO;2.

Salinger, M. J., J. A. Renwick, and A. B. Mullan, 2001: Interdecadal Pacific oscillation and South Pacific climate. *Int. J. Climatol.*, **21**, 1705–1721, https://doi.org/10.1002/joc.691.

Sankaran, A., 2017: Unveiling the multiscale teleconnection between Pacific decadal oscillation and global surface temperature using time-dependent intrinsic correlation analysis. *Int. J. Climatol.*, **37**, 548–558, https://doi.org/10.1002/joc.4713.

Shakun, J. D., and J. Shaman, 2009: Tropical origins of North and South Pacific decadal variability. *Geophys. Res. Lett.*, **36**, L19711, https://doi.org/10.1029/2009GL040313.

Shen, C., W.-F. Wang, W. Gong, and Z. Hao, 2006: A Pacific decadal oscillation record since 1470 AD reconstructed from proxy data of summer rainfall over eastern China. *Geophys. Res. Lett.*, **33**, L03702, https://doi.org/10.1029/2005GL024804.

Shi, H., B. Wang, J. Liu, and F. Liu, 2019: Decadal–multidecadal variations of Asian summer rainfall from the Little Ice Age to the present. *J. Climate*, **32**, 7663–7674, https://doi.org/10.1175/JCLI-D-18-0743.1.

Smith, D. M., and Coauthors, 2016: Role of volcanic and anthropogenic aerosols in the recent global surface warming slowdown. *Nat. Climate Change*, **6**, 936–940, https://doi.org/10.1038/nclimate3058.

Steiger, N. J., J. E. Smerdon, E. R. Cook, and B. I. Cook, 2018: A reconstruction of global hydroclimate and dynamical variables over the Common Era. *Sci. Data*, **5**, 180086, https://doi.org/10.1038/sdata.2018.86.

Steinhilber, F., J. Beer, and C. Fröhlich, 2009: Total solar irradiance during the Holocene. *Geophys. Res. Lett.*, **36**, L19704, https://doi.org/10.1029/2009GL040142.

Stevenson, S., B. Otto-Bliesner, J. Fasullo, and E. Brady, 2016: "El Niño like" hydroclimate responses to last millennium volcanic eruptions. *J. Climate*, **29**, 2907–2921, https://doi.org/10.1175/JCLI-D-15-0239.1.

Sun, C., F. Kucharski, J. Li, F.-F. Jin, I.-S. Kang, and R. Ding, 2017: Western tropical Pacific multidecadal variability forced by the Atlantic multidecadal oscillation. *Nat. Commun.*, **8**, 15998, https://doi.org/10.1038/ncomms15998.

Sun, T., and Y. M. Okumura, 2020: Impact of ENSO-like tropical Pacific decadal variability on the relative frequency of El Niño and La Niña events. *Geophys. Res. Lett.*, **47**, e2019GL085832, https://doi.org/10.1029/2019GL085832.

Tardif, R., and Coauthors, 2019: Last Millennium Reanalysis with an expanded proxy database and seasonal proxy modeling. *Climate Past*, **15**, 1251–1273, https://doi.org/10.5194/cp-15-1251-2019.

Thompson, L. G., T. Yao, E. Mosley-Thompson, M. E. Davis, K. A. Henderson, and P.-N. Lin, 2000: A high-resolution millennial record of the South Asian monsoon from Himalayan ice cores. *Science*, **289**, 1916–1919, https://doi.org/10.1126/science.289.5486.1916.

——, and Coauthors, 2006: Abrupt tropical climate change: Past and present. *Proc. Natl. Acad. Sci. USA*, **103**, 10 536–10 543, https://doi.org/10.1073/pnas.0603900103.

——, E. Mosley-Thompson, M. E. Davis, V. S. Zagarodnov, I. M. Howat, V. N. Mikhalenko, and P.-N. Lin, 2013: Annually resolved ice core records of tropical climate variability over the past ∼1800 years. *Science*, **340**, 945–950, https://doi.org/10.1126/science.1234210.

——, and Coauthors, 2017: Impacts of recent warming and the 2015/2016 El Nino on tropical Peruvian ice fields. *J. Geophys. Res. Atmos.*, **122**, 12 688–12 701, https://doi.org/10.1002/2017JD026592.

——, E. Mosley-Thompson, M. E. Davis, S. E. Porter, D. V. Kenny, and P.-N. Lin, 2018: Global-scale abrupt climate events and black swans: An ice-core-derived palaeoclimate perspective from Earth's highest mountains. *The Himalayan Cryosphere: Past and Present*. N. C. Pant et al., Eds., Special Publication 462, Geological Society London, 7–22, https://doi.org/10.1144/SP462.6.

Vance, T. R., J. L. Roberts, C. T. Plummer, A. S. Kiem, and T. D. van Ommen, 2015: Interdecadal Pacific variability and eastern Australian megadroughts over the last millennium. *Geophys. Res. Lett.*, **42**, 129–137, https://doi.org/10.1002/2014GL062447.

Verdon, D. C., and S. W. Franks, 2006: Long-term behavior of ENSO: Interactions with the PDO over the past 400 years inferred from paleoclimate records. *Geophys. Res. Lett.*, **33**, L06712, https://doi.org/10.1029/2005GL025052.

Vincent, D. G., 1994: The South Pacific convergence zone (SPCZ): A review. *Mon. Wea. Rev.*, **122**, 1949–1970, https://doi.org/10.1175/1520-0493(1994)122<1949:TSPCZA>2.0.CO;2.

Vuille, M., R. S. Bradley, R. Healy, M. Werner, D. R. Hardy, L. G. Thompson, and F. Keimig, 2003: Modeling δ^{18}O in precipitation over the tropical Americas: 2. Simulation of the stable isotope signal in Andean ice cores. *J. Geophys. Res.*, **108**, 4175, https://doi.org/10.1029/2001JD002039.

Wang, S., J. Huang, Y. He, and Y. Guan, 2014: Combined effects of the Pacific decadal oscillation and El Niño–Southern Oscillation on global land dry–wet changes. *Sci. Rep.*, **4**, 6651, https://doi.org/10.1038/srep06651.

Wang, T., O. H. Otterå, Y. Gao, and H. Wang, 2012: The response of the North Pacific decadal variability to strong tropical volcanic eruptions. *Climate Dyn.*, **39**, 2917–2936, https://doi.org/10.1007/s00382-012-1373-5.

Westra, S., B. Renard, and M. Thyer, 2015: The ENSO–precipitation teleconnection and its modulation by the interdecadal Pacific oscillation. *J. Climate*, **28**, 4753–4773, https://doi.org/10.1175/JCLI-D-14-00722.1.

Wise, E. K., 2015: Tropical Pacific and Northern Hemisphere influences on the coherence of Pacific decadal oscillation reconstructions. *Int. J. Climatol.*, **35**, 154–160, https://doi.org/10.1002/joc.3966.

Yan, H., W. Wei, W. Soon, Z. An, W. Zhou, Z. Liu, Y. Wang, and R. M. Carter, 2015: Dynamics of the intertropical convergence zone over the western Pacific during the Little Ice Age. *Nat. Geosci.*, **8**, 315–320, https://doi.org/10.1038/ngeo2375.

Zhang, R., and T. L. Delworth, 2007: Impact of the Atlantic multidecadal oscillation on North Pacific climate variability. *Geophys. Res. Lett.*, **34**, L23708, https://doi.org/10.1029/2007GL031601.

Zhang, Y., J. M. Wallace, and D. S. Battisti, 1997: ENSO-like interdecadal variability: 1900–93. *J. Climate*, **10**, 1004–1020, https://doi.org/10.1175/1520-0442(1997)010<1004:ELIV>2.0.CO;2.

Zhou, X., D. Jiang, and X. Lang, 2020: Unstable relationship between the Pacific decadal oscillation and eastern China summer precipitation: Insights from the Medieval Climate Anomaly and Little Ice Age. *Holocene*, **30**, 1–11, https://doi.org/10.1177/0959683620902215.